# Choroidal Thickness in Early Postnatal Guinea Pigs Predicts Subsequent Naturally Occurring and Form-Deprivation Myopia

Liqin Jiang,[1] Xinyu Liu,[1] Lei Zhou,[1,2] Joanna M. Fianza Busoy,[1] Myo Thu Khine,[1] Yee Shan Dan,[1] Mengyuan Ke,[1] Noel A. Brennan,[3] Karen J. V. Catbagan,[1] Leopold Schmetterer,[1,4] Veluchamy A. Barathi,[1,2] and Quan V. Hoang[1,2,5]

[1]Singapore Eye Research Institute, Singapore National Eye Centre, Duke-NUS Medical School, Singapore
[2]Department of Ophthalmology, Yong Loo Lin School of Medicine, National University of Singapore, Singapore
[3]Johnson & Johnson Vision, Jacksonville, Florida, United States
[4]School of Chemical and Biomedical Engineering, Nanyang Technological University, Singapore
[5]Department of Ophthalmology, Columbia University, New York, New York, United States

Correspondence: Veluchamy A. Barathi, Singapore Eye Research Institute, Singapore National Eye Centre, Duke-NUS Medical School, 20 College Rd, Singapore 169856, Singapore; amutha.b.veluchamy@seri.com.sg. Quan V. Hoang, Singapore Eye Research Institute, Singapore National Eye Centre, Duke-NUS Medical School, 20 College Rd, Singapore 169856, Singapore; donny.hoang@duke-nus.edu.sg.

VAB and QVH contributed equally and share senior authorship.

**Received:** December 7, 2021
**Accepted:** August 19, 2022
**Published:** October 14, 2022

Citation: Jiang L, Liu X, Zhou L, et al. Choroidal thickness in early postnatal guinea pigs predicts subsequent naturally occurring and form-deprivation myopia. *Invest Ophthalmol Vis Sci.* 2022;63(11):10. https://doi.org/10.1167/iovs.63.11.10

**Purpose.** To identify choroidal characteristics associated with susceptibility to development of naturally occurring and experimentally induced myopia.

**Methods.** We compared choroidal properties between pigmented and albino guinea pig (GP) strains. Biometry, cycloplegic refractive error (RE), and eye wall sublayer thickness were measured from 171 GPs at postnatal day (P)6, 14, and 28. Forty-three P14 GPs underwent two-week monocular form-deprivation myopia (FDM). En face images of choroidal vasculature were obtained with a customized swept-source optical coherence tomography. Multivariate regression analyses were performed, with P28 RE as the outcome and P14 choroidal thickness (ChT) as the main predictor variable. Proteomic analysis was performed on choroidal tissue from P14 albino and pigmented GPs.

**Results.** At P14, RE was correlated with thickness of the choroid ($\beta = 0.06$), sclera ($\beta = 0.12$), and retina ($\beta = 0.27$; all $P < 0.001$). P14 ChT was correlated with P28 RE both with ($\beta = 0.06$, $P = 0.0007$) and without FDM ($\beta = 0.05$, $P = 0.008$). Multivariate regression analysis, taking into account FDM (versus physiological growth) and strain, revealed that for every 10-µm greater ChT at P14, P28 RE was 0.50D more positive ($P = 0.005$, n = 70). En face images of choroidal sublayers showed that albino choroids were relatively underdeveloped, with frequent avascular regions. Consistent with this finding, proteomic analysis suggested abnormalities of the nitric oxide system in the albino GP choroid.

**Conclusions.** Current results are consistent with the notion that greater ChT could protect from or delay the onset of myopia, while lower ChT is associated with greater susceptibility to myopia development. The underlying mechanism could be related to dysfunction of the choroidal vascular system.

Keywords: guinea pigs, experimental myopia, choroid, myopia, nitric oxide, sensitivity

It is generally accepted that eye growth is strongly guided by visual signals.[1] Among the components of feedback loops[1] that control the refractive error and eye growth, the choroid plays a pivotal role in the cascade of growth-regulating signals from retina to sclera.[2] The choroid, a vascular layer located between the retina and sclera, consists of multiple blood vessels, with surrounding stromal tissue comprised of nerves, melanocytes, connective tissue, extracellular fluid, and possibly other cell types.

Choroidal thickness (ChT) is not constant but fluctuates with the diurnal cycle[3] and can be altered by different visual stimuli; it was reported initially in chicks that the choroid responded to defocus by spherical lenses,[4,5] and similar responses were detected subsequently in human eyes.[6,7] Therefore a potential role of ChT in dysregulated, myopiagenic eye growth has been intensively studied in humans.[8] Recently, it was reported that the human choroid also responds to astigmatic defocus.[9] Moreover, in human subjects, reading black text on white paper or white text on black paper for a short time period (30 minutes)[10] and narrowband blue or red light exposure[11] induced differential changes in ChT, which were detectable in vivo by monitoring ChT. Animal models are important for understanding the complexity of eye growth and for elucidating signaling pathways in the eye that locally control its functional and physical homeostasis.[12] Based on studies in chicks, it is well accepted that changes in ChT displace the retina, moving the photoreceptors toward (under positive defocus) or away from (under negative defocus) the plane of focus.[4,5,13,14] This bidirectional modulation of axial elongation might allow for eyes to grow toward functional emmetropia[15] because the choroid becomes thinner during faster eye growth and

thicker during slower eye growth. Studies on ChT in chickens have found that ChT in untreated eyes was variable,[16] but it was not associated with the susceptibility to form deprivation myopia (FDM).[17] Later it was confirmed by Nickla and Totonelly,[18] who reported more extensive data not only from FDM, but also from plus and minus lens-induced defocus and drug treatments. ChT has also been shown to be variable among individual children[19] and to vary with age. For example, Read and colleagues[20] reported that ChT increased with age from 4 to 12 years, and Wakatsuki et al.[21] reported that ChT decreased with age from 20s to 70s. Similarly, a longitudinal, population-based observational study in humans by Hansen et al.[22] concluded that thinness of the subfoveal choroid at age 11 years did not predict the axial eye elongation and incident myopia from age 11 to 16 years; however, their reported ChT at age 11 years was 361 ± 77 µm—which is thicker than the average ChT reported among emmetropic children at comparable ages among Australian,[20] Chinese,[23] and Turkish children.[24] In addition to the fact that myopia in human children and growing guinea pigs undoubtedly differs on many grounds, given the imperfection of any animal model of disease, it is worth noting that a ChT of 361 ± 77 µm is thicker than that found in emmetropic human eyes. Thus it may not have been in the range typical of myopic children but rather within the range suggested to be protective against myopia development in guinea pigs (GPs), if our previous findings in GPs are directly translatable to human children.[14]

Despite significant differences in eye structure between birds and mammals, the mammalian choroid has a similar ability to respond to certain visual conditions by becoming thinner or thicker. Therefore we used the GP as a mammalian model to elucidate whether ChT is a reflection of choroidal function and whether it can predict susceptibility to myopia development (either spontaneously or in response to FDM) later in life. In the current study we use albino GPs, more than 50% of which develop myopia spontaneously[25]—together with the strain of Elm Hill-sourced pigmented GPs, which have been reported to have thicker choroids and to be more resistant to experimentally-induced monocular FDM[14]—to determine which choroidal characteristics are associated with susceptibility to the induction of myopia. We then further explored the effects of differences in ChT on eye growth—at baseline (before starting treatments) and without and with the addition of myopiagenic optical conditions. Thus the aims of the current study were (1) to explore the potentially causative contributions of the choroid to refractive development and (2) to provide further evidence that tissue components in the choroid are associated with susceptibility to myopia-induction.

## Materials and Methods

### Animals and Housing

Both pigmented and albino GPs were used in the current study. Breeders were purchased from a commercial supplier (Elm Hill Labs, Chelmsford, MA, USA) and bred on site. Groupings for breeding were restricted to unrelated animals, based on on-site records. Usually, pups would stay with parents until weaning at day 21; they would then be housed as same-sex pairs in transparent plastic wire-top cages, in a room with 12-hour/12-hour light/dark cycle and average floor luminance of approximately 160 to 180 lux (Fluorescent light with 65% White light, PHILIPS, TL5/28W/840 [4 Feet], Koninklijke Philips N.V., Amsterdam, Netherlands). Animals had free access to water and vitamin C–supplemented food, and they received fresh fruits and vegetables at least three times a week as dietary enrichment. All animal care and treatments in this study conformed to the ARVO Statement for the Use of Animals in Ophthalmic and Vision Research. Experimental protocols were approved by the Institutional Animal Care and Use Committee of SingHealth (AAALAC Accredited; 2018/SHS/1441).

### Myopia Induction and Measurements of Ocular Parameters

Myopia was induced by placing a diffuser over the treated eye (left or right, assigned at random), with the fellow eye remaining untreated to serve as an internal reference. Pups destined for form deprivation were weaned at postnatal day 10 (P10) and then fitted with a diffuser at P14, as described by Howlett and McFadden.[26] In brief, two pieces of loop-side Velcro arcs were glued above and below the eyelids; then a diffuser, mounted on a matching hook-side Velcro ring, was attached to the arcs, and the animals were single-housed for two weeks. Pups designated as normal-normal control stayed with parents until weaning at P21 and were then housed as same-sex pairs.

Eye growth in pups of both strains (with or without FDM) was monitored weekly, starting at P6. Only data from right eyes of pups undergoing normal growth were included. Refraction data were collected using streak retinoscopy and reported as spherical equivalent refractive error. Cycloplegic retinoscopy with trial lenses was performed in the morning in awake animals hand-held, 30 minutes after topical application of 1% cyclopentolate hydrochloride (Bausch & Lomb, Rochester, NY, USA), at P6, P14, and P28. The precision of measurement was controlled as ±0.25D. After retinoscopy, axial length (AL) and vitreous chamber depth (VCD) were measured using A-scan ultrasonography (10 MHz PacScan 300A; Sonomed Escalon, New Hyde Park, NY, USA) in awake animals with local corneal anesthesia (0.5% Alcaine eye drop; Alcon, Geneva, Switzerland). For optical coherence tomography (OCT) imaging, all scanning was performed in the late afternoon around 5 PM, to minimize variability caused by circadian fluctuations in ChT. Animals were anesthetized by intramuscular injection of a cocktail of ketamine hydrochloride, 27 mg/kg (ketamine; Ceva Animal Health, Lenexa, KS, USA) and xylazine hydrochloride, 0.6 mg/kg (Ilium Xylazil-20; Troy Laboratories, Glendenning, NSW, Australia) for routine fundus imaging, and a higher dose of 45/5 mg/kg ketamine/xylazine cocktail was used when imaging was repeated within two hours. Spectral domain optical coherence tomography (SD-OCT; Spectralis HRA+OCT; Heidelberg Engineering, Heidelberg, Germany) was used to acquire high-resolution anterior segment images with the anterior segment module, and posterior segment imaging was performed by attaching a 55° wide-angle lens with the Spectralis Widefield Imaging Module. All images were evaluated by using Heidelberg Eye Explorer software (HEYEX, version 1.7.1.0) and measuring with built-in digital calipers. In the FDM experiments, the same sequence was followed, and all measurements were performed at baseline (P6 and P14), and after two additional weeks with or without unilateral form-deprivation.

Investigative Ophthalmology & Visual Science

### SD-OCT Image Acquisition and Analysis

SD-OCT scans of the anterior segment were acquired at high resolution along the temporal-nasal direction. Images included the limbus and equal lengths of the iris on both sides. Anterior chamber depth was measured midway between the limbus of the two sides, and at the middle of the iris (for anatomical reference); the mean of three measurements was taken as the final value. Corneal central thickness (CCT) was measured.

SD-OCT scans of the posterior segment were also acquired at high resolution with the Spectralis Widefield Imaging Module with eye-tracking (TruTrack). All images were taken with 13 B-scan lines, and axial A-scan resolution was 1536 pixels per line. Scanning started from the upper edge of the optic nerve head (ONH) and continued superiorly across the visual streak. The enhanced depth imaging mode was turned on, and 15 frames of images were registered for each B-scan line. The thicknesses of the retina, choroid, and sclera were measured repeatedly over time. Images from the visual streak area were processed as described previously[14]; in brief, images were selected from the visual streak area, which is approximately 2.5 ONH diameters above the center of the ONH, and the thickness of each sublayer was measured 10 times for all selected images.

### Swept Source-OCT (SS-OCT) Choroid Imaging

The three-dimensional structure of the retina was examined with a customized high-speed SS-OCT,[27] which used a swept source of wavelengths centered at 1050 nm, with an A-scan rate of 200 kHz. The high scanning rate allowed for a volume scan of the retina and choroid with minimal motion artefacts. The scan, which was centered anatomically on the ONH, covered an area of 4 × 4 mm with 1000 × 1000 A-scans.

Eyes were imaged on P6 and P14, and serial OCT B-scans were obtained in the anterior-posterior plane. These two-dimensional cross-sectional B-scan images were combined to create a three-dimensional volume image, which was then virtually flattened so that the retinal pigment epithelium (RPE) layer was a single plane, located by definition at 0 µm, using a script coded in MATLAB (2020b; MathWorks, Inc., Natick, MA, USA). After flattening, the volume image was resliced in the horizontal (en face) plane. Using the RPE layer as a landmark, en-face images of inner, middle, and outer choroid were selected, at distances of 10 µm, 20 µm, and 50 µm posterior to the RPE, respectively.

### Proteomic Analysis

Freshly enucleated eyes from P14 GPs were placed on ice, the anterior segment was removed via a circumferential perilimbal incision, and then the lens, vitreous, and retina were gently removed. Next, each eyecup was radially cut and flattened, and the whole choroid (with some remaining RPE) was scraped from the sclera. Then the choroidal tissue was carefully picked up using fine dissecting tweezers, placed in a 1.5 mL tube, flash-frozen in liquid nitrogen, and stored at −80°C until used for iTRAQ-based quantitative proteomics analysis. Choroidal tissues from the right eyes of four albino and four pigmented P14 GPs were used for iTRAQ 8-plex experiments.

Briefly, for the iTRAQ 8-plex experiments, each choroidal tissue sample was homogenized, and lysis buffer was applied (iST kit; PreOmics, Bayern, Germany). The tissue lysates were then spun in a centrifuge at 16,000*g* for 10 minutes at 4°C. The supernatants of the respective tissues were collected for protein quantitation using DC Protein Assay (Bio-Rad Life Science, Hercules, CA, USA). Protein solutions were then reduced, alkylated, digested, and cleaned up according to the manufacturer's instructions (iST kit; PreOmics). Each peptide concentration was determined with a Pierce Quantitative Fluorescent Peptide Assay (Thermo Fisher Scientific, Waltham, MA, USA). Subsequently, each peptide solution (100 µg of total peptide) was labeled with the iTRAQ 8-plex Label Reagent (SCIEX, Framingham, MA, USA) according to the manufacturer's protocol and fractionated into 10 fractions by high-pH LC using a Waters HPLC system (Waters Ltd, Elstree, UK). Each one of these 10 fractions was reconstituted in 0.1% formic acid + 5% acetonitrile and analyzed using an Ultimate 3000 nanoLC system (Thermo Fisher Scientific) coupled with a TripleTOF 5600 (SCIEX). The resulting MS/MS data were processed using ProteinPilot 5.0 software (SCIEX), and the iTRAQ data were searched for matches in the Guinea pig Uniprot Reference Proteome (which contains 32,019 proteins).

The linear models for microarrays (limma) algorithm[28] was used to assess the significance of different content of dysregulated proteins (albino GP vs. pigmented GP). The relative amounts of dysregulated proteins (albino GP vs. pigmented GP) were defined as fold change >1.5 and $P < 0.05$ (moderated *t*-test) for up-regulated proteins, or fold change <0.67 and $P < 0.05$ (moderated *t*-test) for down-regulated proteins.

The list of up-regulated and down-regulated proteins was uploaded to QIAGEN's Ingenuity Pathway Analysis (IPA) software and database (Qiagen, Germantown, MD, USA) for core analysis to identify the canonical pathways that were significantly different in albino versus pigmented GP choroid. IPA Core Analysis module was used to predict the effects of protein level changes in the datasets on biological processes derived from the literature compiled in the Ingenuity Knowledge Base. The Expression Analysis examines proteins in the dataset that are known to affect functions, compares the proteins' direction of change to expectations derived from the literature, and then issues a prediction for each function based on the direction of change. The direction of change was determined as the difference in choroidal protein levels in albino versus pigmented GPs. We used the Fisher's exact test with a *P* value threshold of 0.05 to estimate statistical significance, and the z-score algorithm to make predictions about direction of change. The activation z-score was used to infer likely activation states of biological functions based on comparison with a model that assigns random regulation directions. The activation z-score was also used in the IPA Pathways Activity Analysis module to predict activation or suppression of the canonical pathways affected by GP strains.

### Statistics

All data groups were analyzed for normality of distribution and equality of variance by the Anderson-Darling and Kolmogorov-Smirnov tests, using GraphPad Prism 8.0.0 for Windows (GraphPad Software, San Diego, California USA, www.graphpad.com), and the outcomes were used to determine whether parametric or nonparametric statistical analyses were appropriate. Before treatment, animals (Table 1, Group 1, n = 51) were divided into three subgroups according to their manifest refractive error at P6: hyperopic albino (n = 17), myopic albino (n = 17), and hyperopic pigmented (n = 17). All data sets passed the normality test,

**Table 1.** Summary of Sample Size and Statistical Methods Used for Main Analyses (Total Sample Size: n = 171 Animals)

| | Albino | Pigmented | Statistics |
|---|---|---|---|
| Group 1 (G1) (Fig. 1) | hyperopic: n = 17<br>myopic: n = 17 | hyperopic: n = 17 | One-way ANOVA with Bonferroni correction |
| Group 2 (G2) (Figs. 2, 3) (Tables 2, 3) | n = 27 | n = 23 | One-way ANOVA with Bonferroni correction; Correlation analysis |
| Proteomics analysis (Fig. 7, Table 4) | n = 4 from G2 | n = 4 from G2 | Linear models for microarrays algorithm (limma) |
| Group 3 (G3) FDM from 2 to 4 weeks of age (Fig. 4) | Control: n = 17<br>FDM: n = 22 | Control: n = 10<br>FDM: n = 21 | Correlation analysis; Multivariate linear regressions |
| Repeated ChT measurement (Fig. 5) | n = 7 from G3 | n = 7 from G3 | One-way ANOVA with Bonferroni correction |

Group 1 guinea pigs were used for cross-sectional, case-control comparisons at P6. After guinea pigs were recruited, they underwent biometric measurements and optical coherence tomography imaging. Group 2 guinea pigs were observed longitudinally from P6 to P14 to assess the correlation between ChT and refraction. Group 3 guinea pigs either underwent FDM induction or served as age-matched controls that underwent natural eye growth. Only the right eyes from guinea pigs undergoing natural growth were included in analyses. FDM was induced in either left or right eye (assigned at random). Of the n = 27 albinos in Group 2, based on P6 baseline refraction, four were myopic, and 23 were hyperopic; whereas at P14 refraction, more GPs naturally progressed to myopia, with 12 myopic, 2 emmetropic and 13 still hyperopic. Of the n = 22 albinos that underwent FDM in Group 3, at P14 baseline refraction, there were seven myopic, one emmetropic, and 14 hyperopic animals.

so the biometric parameters in these three subgroups were compared using one-way ANOVA, followed by Bonferroni correction when necessary. All data are reported as mean ± standard error.

To interpret our results further, we tested for associations between the absolute refraction at P6 and the thickness of fundal sublayers in a separate group of GPs (Table 1, Group 2, n = 50; right eyes of 27 albino and 23 pigmented GPs) by computing correlation coefficients and displaying the results in scatterplots. We then similarly tested the association between the absolute refraction at P14 and the same fundal sublayer thicknesses. Measurements were made initially at P6 and followed up at P14 in four pigmented and four albino GPs that were euthanized subsequently for proteomics analysis.

The same methods were used to test for associations between absolute ChT at P14 (baseline) and refraction at P28, with and without form deprivation (Table 1, Group 3, n = 70). Additionally, multivariate linear regressions were performed with P28 refractive error as the outcome variable and P14 ChT as the main predictor variable, to test further for a potential role of ChT on myopic eye growth. These multivariate linear regressions allow us to control for (account for) various potential confounding variables, including strain (pigmented vs. albino) and the induction of form-deprivation myopia (FDM vs. control eyes undergoing normal, physiologic (untreated) growth). Only one eye was analyzed from a given GP; therefore "control" eyes were from control GPs in which neither eye underwent FDM. For all data analyses, differences with p-values less than 0.05 were considered statistically significant. Sample sizes and statistical methods are summarized in Table 1.

## Results

### Differences in Biometric Parameters Between Strains, without Induced Myopia

To evaluate strain-dependent differences in refraction, biometric parameters in the eyes of pigmented and albino GPs were compared in detail. Our results showed that eye sizes were similar in the two strains (Fig. 1A) but revealed substantial differences in the thicknesses of eyewall sublayers (Fig. 1B). At baseline (P6), the eyes of the pigmented strain were consistently hyperopic (6.1 diopters (D) ± 3.4D; statistically significantly different from those in albinos, F (2, 48) = 65.7; $P < 0.001$, Fig. 1A inset). In addition, our results showed that each part of the eyewall was significantly thicker in pigmented eyes than in albino eyes (one-way ANOVA: retina, F (2, 48) = 10.4, $P < 0.001$; choroid, F (2, 48) = 177.9, p < 0.001; sclera, F (2, 48) = 9.7, $P < 0.001$; CCT, F (2, 48) = 23.9,

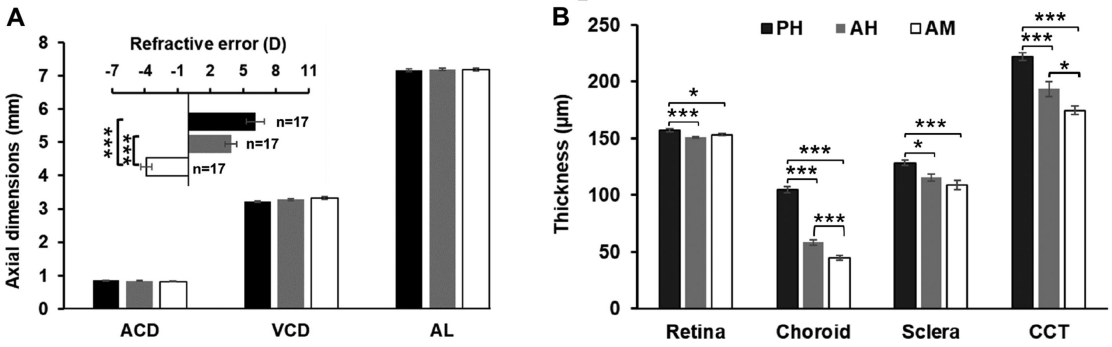


**Figure 1.** Comparisons of baseline biometric data between strains with distinctive refractions at P6 (**A, inset**). (**A**) Anterior chamber depth (ACD), VCD, AL, and refractive error (in diopters, D) for the three different strains. (**B**) Thicknesses of each layer of the eye wall, in the different refractive groups. PH, pigmented, hyperopic; AH, albino, hyperopic; AM, albino, myopic. Statistical comparisons: *$P < 0.05$; ***$P < 0.001$, with Bonferroni correction after one-way ANOVA.

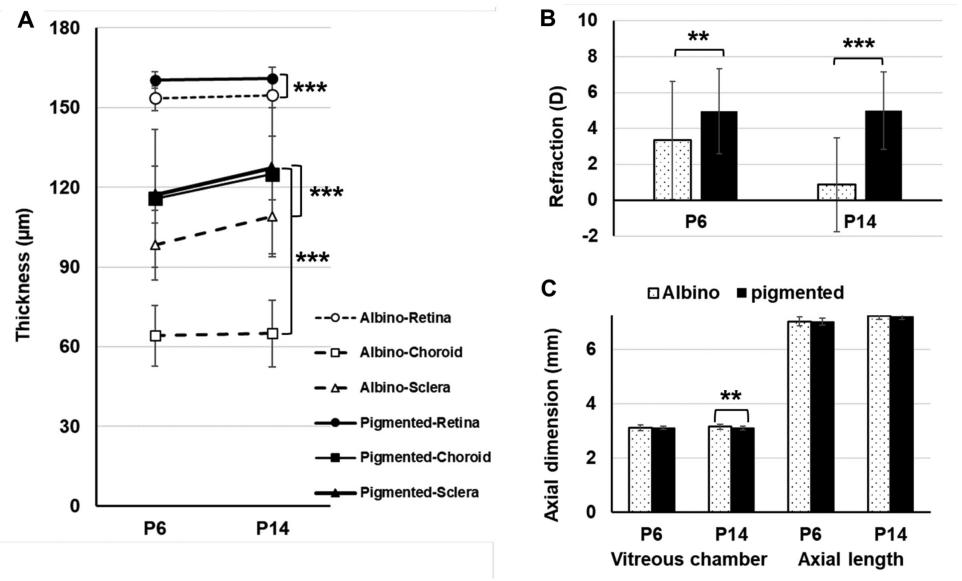


**Figure 2.** Longitudinal changes, from P6 to P14, in thickness of the fundus sublayers within the visual streak area (**A**), refraction (**B**), and axial dimensions of the eye (**C**), in both albino and pigmented GPs. Statistical comparisons: $^{**}P < 0.01$; $^{***}P < 0.001$, with Bonferroni correction after one-way ANOVA.

$P < 0.001$, Fig. 1B), regardless of whether they were hyperopic (albino-hyperopia, 3.9D ± 2.3D) or myopic (albino-myopia, −3.9D ± 2.2D, Fig. 1A inset). With Bonferroni correction, the difference in refractions between pigmented and albino hyperopic groups was marginally significant ($P = 0.051$, Fig. 1A inset). However, we found significant differences in ChT (58.4 ± 9.8 µm vs. 44.5 ± 8.5 µm; $P < 0.001$) and CCT (193.4 ± 26.7 µm vs. 174.6 ± 16.6 µm; $P = 0.026$) between albino-hyperopia and albino-myopia GPs (Fig. 1B).

## Biometric Parameters and Posterior Eye Wall Layer Thickness Vary as a Function of Refractive Development in Naturally-Occurring Myopia (Without FDM)

Longitudinal observations from P6 to P14 showed that the absolute thicknesses of the layers of the eye wall in pigmented GPs were significantly different from those in albinos at both time points (Fig. 2A). Although retinal thickness did not change significantly from P6 to P14 in either strain, the sclera thickened significantly over that time in both strains ($P < 0.0001$). Interestingly, ChT at both time points (P6 and P14) was significantly less in albinos than in pigmented GPs, and the choroid thickened significantly with age from P6 to P14 ($P < 0.0001$), in pigmented but not in albino GPs. At P6 baseline, refractions in the two strains were significantly different, but vitreous chamber depths were similar (Figs. 2B, 2C). Later, at P14, the difference between refractions in the two strains had increased; the vitreous chamber elongated with age in albino eyes, but it remained unchanged with age in pigmented eyes (Figs. 2B, 2C). Details of all biometric parameters are listed in Table 2.

Of note, ChT varied greatly (large standard deviation [numbers in bold in Table 2] indicated wide range of ChT, larger than the standard deviation of the relatively thicker retina) in both albino (42-86 µm) and pigmented (65-182 µm) eyes at age P6, and this variation increased slightly with age (P14) in both albino (42-95 µm) and pigmented (72-207 µm) eyes. Therefore the association of ChT at P14 with myopia development at P28 (with or without monocular form deprivation) was evaluated in the "Association of P14 Baseline ChT With P28 Refractive Error" section below.

**Table 2.** Biometric Parameters (Refraction, Axial Length, and Component Distances) of Eyes Undergoing Normal Growth at Two Baseline Time Points (P6 and P14)

| | Albino Strain (n = 27) | | Pigmented Strain (n = 23) | |
|---|---|---|---|---|
| **Parameters*** | **P6** | **P14** | **P6** | **P14** |
| Refraction (D) | 3.3 ± 3.0 | 0.6 ± 2.5 | 4.6 ± 2.2 | 5.0 ± 2.2 |
| Axial length (mm) | 7.06 ± 0.2 | 7.28 ± 0.1 | 7.04 ± 0.1 | 7.21 ± 0.1 |
| Vitreous chamber (mm) | 3.13 ± 0.1 | 3.19 ± 0.1 | 3.13 ± 0.0 | 3.12 ± 0.1 |
| Retina (µm) | 154 ± 4 | 154 ± 5 | 161 ± 3 | 161 ± 4 |
| Choroid (µm) | 64 ± **11**† | 64 ± **13**† | 116 ± **27**† | 125 ± **31**† |
| Sclera (µm) | 98 ± 13 | 109 ± 14 | 117 ± 9 | 127 ± 12 |

All values represent mean ± standard deviation.
* Only the data from right eyes were used.
† Note the standard deviation tended to be greater in P14 versus P6 GPs.

**Table 3.** Correlation Analysis Showing Coefficient of Correlation of Refractive Error With Thickness of Each Sublayer of the Posterior Eye Wall, at P6 and P14

| | P6 (n = 50) | | P14 (n = 50) | | P6 Albino (n = 27) | | P6 Pigmented (n = 23) | | P14 Albino (n = 27) | | P14 Pigmented (n = 23) | |
|---|---|---|---|---|---|---|---|---|---|---|---|---|
| | $\beta$ | ***P*** | $\beta$ | ***P*** | $\beta$ | ***P*** | $\beta$ | ***P*** | $\beta$ | ***P*** | $\beta$ | ***P*** |
| Retinal thickness | 0.145 | 0.06 | 0.272 | **0.0002*** | 0.18 | 0.24 | −0.001 | 0.99 | 0.102 | 0.35 | 0.094 | 0.35 |
| Choroidal thickness | 0.022 | 0.06 | 0.022 | **<0.0001*** | −0.05 | 0.37 | 0.033 | **0.06** | 0.069 | **0.09** | 0.041 | **0.0013*** |
| Scleral thickness | 0.050 | 0.06 | 0.118 | **<0.0001*** | 0.004 | 0.93 | 0.141 | **0.006*** | 0.036 | **0.032*** | 0.049 | 0.72 |

Only the data from right eyes were used. *P* values indicate the significance of deviation of the slopes from zero. Bold font alone denotes values close to statistical significance, at $0.10 > P > 0.05$. Asterisk and bold font implies significance at $P < 0.05$.

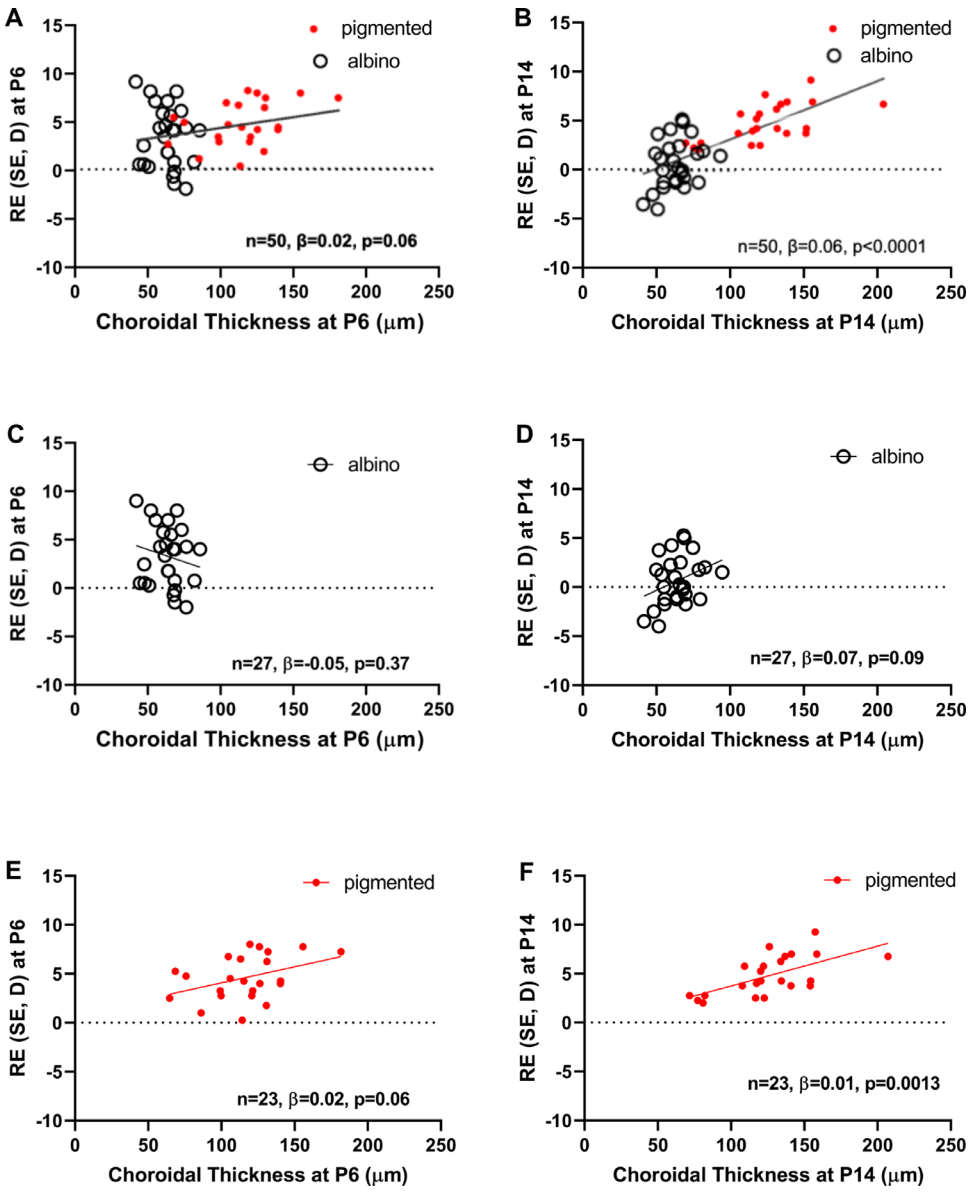


**Figure 3.** Association between choroidal thickness and refraction at P6 (**A, C, E**) and P14 (**B, D, F**) when the two guinea pig strains were combined (**A, B**) and analyzed with strains separated (**C, D, E, F**). $\beta$, regression coefficient; D, diopters; SE, spherical equivalent.

Associations between refraction and the thickness of each eye-wall sublayer were analyzed at P6 and P14. The correlation coefficients are listed in Table 3. All three associations became stronger with age, in both albino and pigmented animals, but the association of ChT with refraction at P14 was the strongest. Scatter plots of refraction versus ChT are presented in Figures 3A (P6) and 3B (P14). We found a significant positive correlation at P14 ($n = 50$, $\beta = 0.06$, $P < 0.0001$) and a marginally significant positive correlation at P6 ($n = 50$, $\beta = 0.02$, $P = 0.06$).

Investigative Ophthalmology & Visual Science

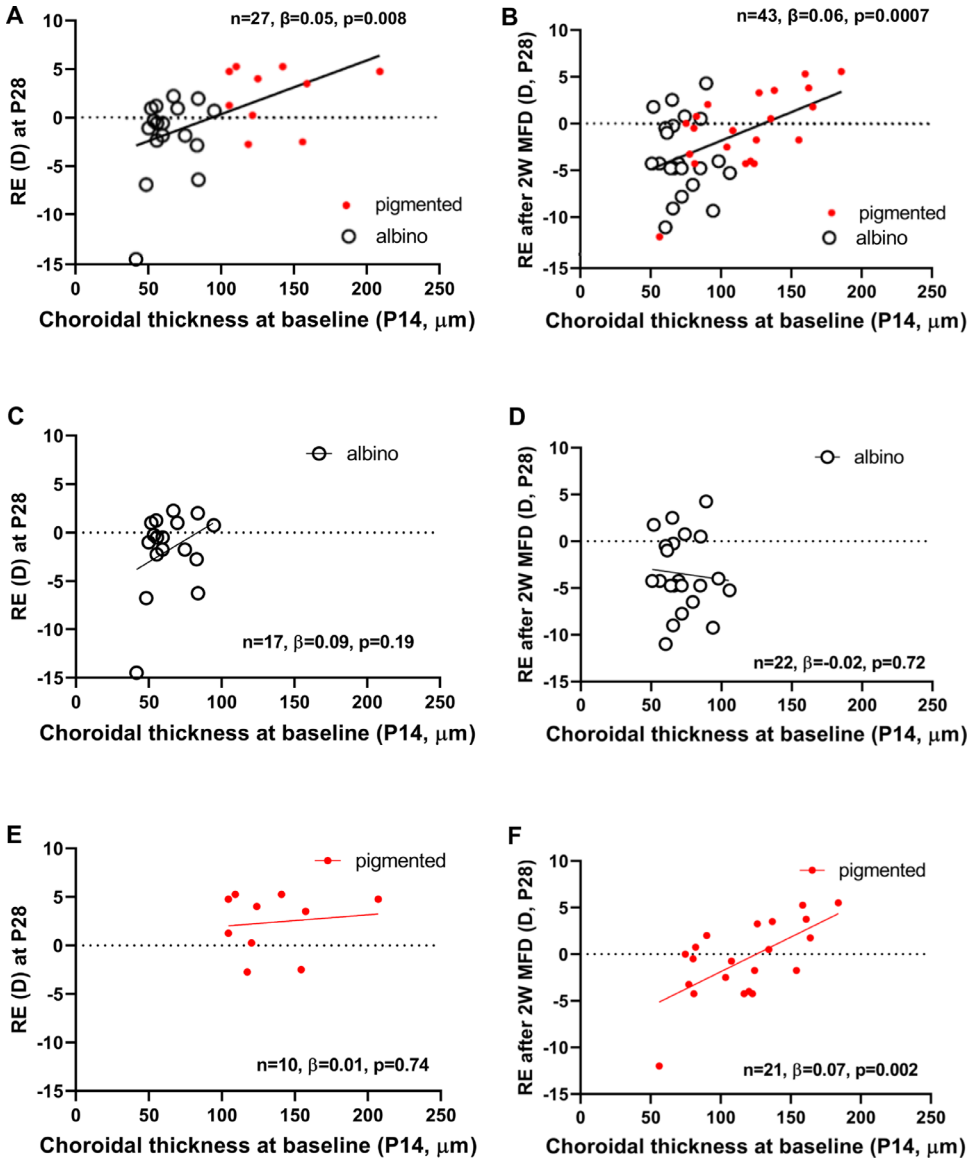


**Figure 4.** Association between choroidal thickness at baseline (P14, x-axis) and refractive error at P28 (RE, y-axis), after 14 days of either normal growth (**A, C, E**) or form deprivation (**B, D, F**) when the two guinea pig strains were combined (**A, B**) and when analyzed with strains separated (**C, D, E, F**). These strong associations (r = 0.50) indicate that baseline choroidal thickness could predict susceptibility to myopia development. 2W MFD, two weeks of monocular form deprivation myopia inducement; $\beta$, regression coefficient; D, diopters.

Next, we assessed whether the relationship between ChT and refractive error (at P6 and at P14) varied across albino and pigmented GPs (Table 3, Fig. 3). At P6, we found that the correlation in albino GPs was negative and not significant, (n = 27, $\beta = -0.05$, $P = 0.37$, Fig. 3C), whereas the correlation was positive and marginally significant for the pigmented group (n = 23, $\beta = 0.02$, $P = 0.06$, Fig. 3E), implying that the observed positive relationship between P6 ChT and P6 refractive error in the overall sample was driven by pigmented GPs. At P14, we found that the correlation in albino GPs was positive and marginally significant, (n = 27, $\beta = 0.07$, $P = 0.09$, Fig. 3D) and the correlation was positive and significant for the pigmented group (n = 23, $\beta$ = 0,01, $P = 0.0013$, Fig. 3F), implying that the observed positive relationship between P14 ChT and P14 refractive error in the overall sample may be driven more by pigmented GPs than albino GPs.

## Association of P14 Baseline ChT With P28 Refractive Error

At P14 baseline, ChT was lower in albinos than in pigmented GPs (64 ± 13 μm vs. 125 ± 31 μm, $P < 0.001$) (Fig. 2, Table 2), but the ranges of thickness in the albino (40-106 μm) and pigmented (65-207 μm) GPs overlapped somewhat (Fig. 3). After monocular form deprivation for 14 days (n = 22 albino and n = 21 pigmented), the induced myopic shift in refraction was correlated with baseline P14 ChT. In both albino and pigmented GPs with significantly lower baseline ChT, the mean refractive error was significantly myopic after 14 days of form deprivation (Fig. 4). This demonstrates a significant association between ChT and the subsequent development of induced form deprivation myopia.

The relationship between P14 ChT and P28 refractive error was analyzed further by linear regression (Fig. 4).

Univariate linear regression analysis with P28 refractive error as the outcome variable and FDM (versus control) as the predictor variable, showed that if a P14 GP underwent 2 weeks of FDM, at P28 the refractive error was on average 1.85D more myopic than that in GPs undergoing physiological growth; this difference was not quite significant statistically ($P = 0.081$, n = 70). When using P14 baseline ChT as the predictor variable, every additional 10µm of P14 ChT was associated with 0.55D more positive P28 refractive error ($P < 0.001$, n = 70, same data as used for Fig. 4).

We showed, using multivariate linear regression analysis, that after taking into account whether a GP was undergoing FDM (versus undergoing physiological growth), or was albino (versus pigmented), refractive error at P28 was 0.5D more positive with every 10µm increase in ChT at P14 ($P = 0.005$, n = 70). This suggests that the observed relationship between P14 baseline ChT and P28 refractive error is not driven by average differences across albino and pigmented GPs in P14 baseline ChT (same data as used for Fig. 4).

Next, we assessed whether the relationship between P14 baseline ChT and P28 refractive error (with physiologic growth, Fig. 4A, and with two- week FDM, Fig. 4B) varies across albino and pigmented GPs. Specifically, we repeated the analysis using albino GPs (Figs. 4C and 4D) and pigmented GPs (Figs. 4E and 4F). We found that P14 baseline ChT was predictive of P28 refractive error with both physiological growth (n = 27, $\beta = 0.05$, $P = 0.008$) and after two weeks of FDM (n = 43, $\beta = 0.06$, $P = 0.007$). When focusing on P28 refractive error with physiological growth, and analyzing the data from the two strains separately, we found a positive correlation in albino GPs, as well as a positive correlation in pigmented GPs, but neither correlation was statistically significant, although with notably lower sample sizes. When focusing on P28 refractive error after two weeks of FDM, we found that the correlation in albino GPs was near zero and not significant, (n = 22, $\beta = -0.02$, $P = 0.72$), whereas the correlation was positive and statistically significant for the pigmented group (n = 21, $\beta = 0.07$, $P = 0.002$), implying that the observed positive relationship between P14 baseline ChT and P28 refractive error in the overall sample is driven by pigmented GPs.

## Differences in Development of Choroidal Vasculature and Nitric Oxide (NO) Systems Between Pigmented and Albino Animals

**Refractive Error Differences Between Strains.** Stratifying by FDM versus control, among control GPs undergoing physiological growth (GPs contained within Fig. 4A), albino GPs were on average 4.14D more myopic than pigmented GPs ($P = 0.012$, n = 27); in contrast, among GPs that underwent two weeks of FDM (GPs contained within Fig. 4B), albino GPs were on average 2.86D more myopic than pigmented GPs ($P = 0.026$, n = 43). Univariate linear regression analysis, using albino (versus pigmented) strain as the predictor variable, revealed that at P28 albino GPs had a refractive error on average 3.08D more myopic than pigmented GPs ($P = 0.02$, n = 70, combining data from all GPs contained within Figs. 4A and 4B). Notably, after taking into account whether FDM was induced or not, multivariate linear regression analysis showed that albino GPs were on average 3.33D more myopic than pigmented ($P = 0.001$, n = 70, combining data from all GPs contained within Figs. 4A, 4B).

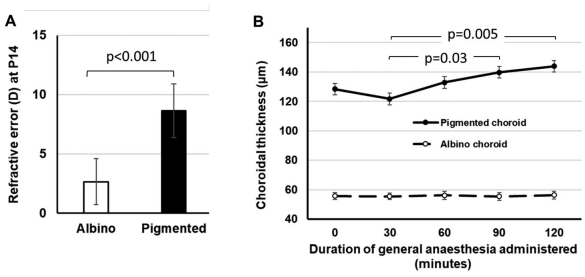


**Figure 5.** Initial refractive error and changes in choroidal thickness with duration of general anesthesia, in P14 hyperopic guinea pigs. (**A**) Refraction of albino and pigmented strains; (**B**) Choroidal thickness as a function of time. Independent Student's *t*-test was used for comparisons in **A**. One-way ANOVA with Bonferroni correction was performed for the data in **B**.

**Choroidal Vasculature Differences Between Strains.** The initial ChT of seven hyperopic albino (2.64D ± 1.94D) and seven hyperopic pigmented (8.64D ± 2.27D) P14 GPs was monitored with the GPs under general anesthesia for two hours. As expected, the initial hyperopic refraction (Fig. 5A) and ChT (Fig. 5B) were remarkably higher in pigmented GPs than in albinos. Of note, ChT increased with the duration of anesthesia in the pigmented GPs, and at least one of the increases was statistically significant at different time points, in pigmented (one-way ANOVA, F = 4.9, $P = 0.004$) but not in albino GPs (F = 0.03, $P = 0.99$). Post hoc test with Bonferroni correction showed that the specific timepoints at which ChT was different, were at 90 minutes versus 30 minutes ($P = 0.03$), and at 120 minutes versus 30 minutes ($P = 0.005$) after anesthesia induction in pigmented GPs. Images of the inner, middle and outer sublayers of the choroid showed that albino GPs have thinner choroids than pigmented GPs, with a relatively underdeveloped vascular layer (Fig. 6; regions with sparse vessels are denoted by stars in the *en face* images).

This inter-strain difference was further explored by linear regression analysis. Univariate linear regression analysis, using P14 baseline ChT as the predictor variable, every additional 10 µm of P14 ChT was associated with 0.64D more positive P28 refractive error ($P < 0.001$, n = 31) in albino GPs, but there was no significant association in pigmented GPs (coefficient 0.10D, $P = 0.814$, n = 39).

**Choroidal Nitric Oxide System Differences Between Strains.** The iTRAQ-based quantitative proteomics analysis was performed, to compare the choroidal proteomes in P14 albino GPs with those in P14 pigmented GPs. The volcano plot in Figure 7 represents fold changes (albino vs. pigmented, $\log_2$) of the same proteins against the moderated *t*-test *P* value ($-\log_2$). In total, 5600 unique proteins were identified (FDR < 1%), 5457 of which were quantifiable; 377 of these were increased in amount, and 282 were decreased (fold change >1.5, or <0.67, *P* value <0.05). All of the differentially expressed proteins were subjected to Ingenuity Pathway Analysis (Qiagen IPA; Supplementary Table S1).

Nitric oxide (NO) subserves many functions in neural and non-neural tissues. As a vasodilator, it is a pivotal signaling molecule that regulates blood flow and tissue oxygenation, and is possibly the most relevant chemical modulator of ChT.[29] It is also an important modulator of functional

Investigative Ophthalmology & Visual Science

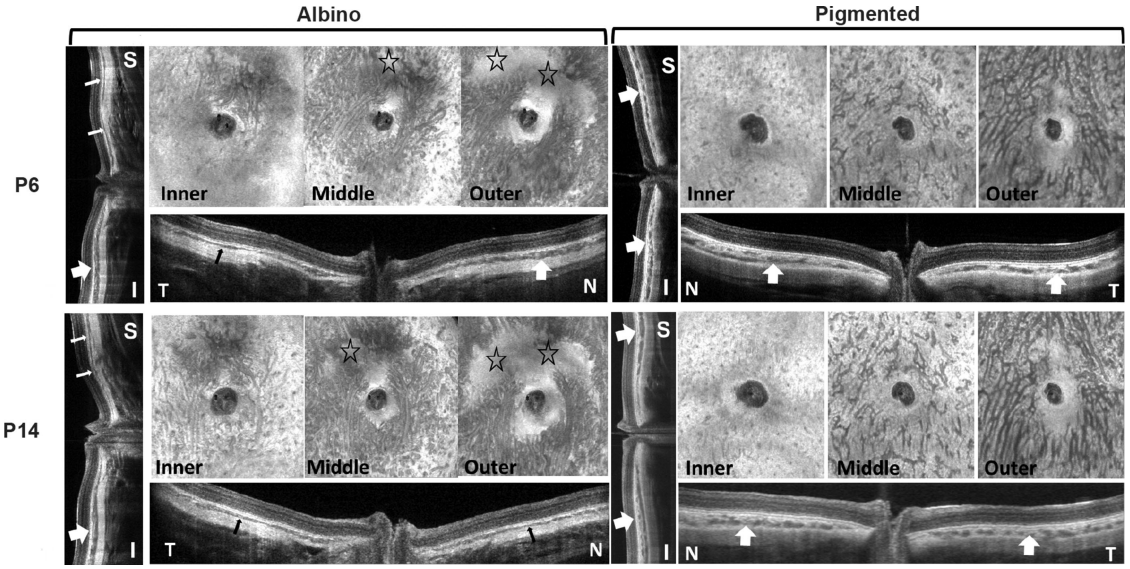


**Figure 6.** En face and cross-sectional images from representative pigmented and albino GP eyes at P6 (**upper images**) and P14 (**lower images**) showing the development of vascular layers of the choroid. S, superior; I, inferior; T, temporal; N, nasal. *Stars* denote underdeveloped choroidal areas in the albino eye. All images were obtained by SS-OCT. *Thin arrows* indicate thin choroid, and *thick arrows* indicate thick choroid—showing the unevenness of ChT in albino GPs and more even ChT in pigmented GPs in different quadrants.

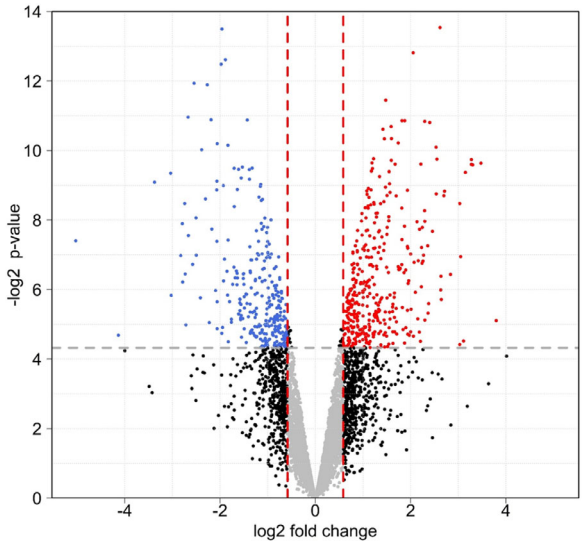


**Figure 7.** Volcano plot for comparison of choroid proteomes between albino P14 GP (n = 4) and pigmented P14 GP (n = 4). Expression fold changes (albino vs. pigmented, $\log_2$) were calculated and plotted against the moderated *t*-test *P* value ($-\log_2$). In total, 5600 unique proteins were identified (FDR < 1%), 5457 of which were quantifiable. Amounts of 377 proteins were increased, whereas amounts of 282 were decreased (fold change > 1.5, or < 0.67; $P < 0.05$). The affected proteins were subjected to Ingenuity Pathway Analysis (Supplementary Table S1).

state and cell-cell signaling (e.g., in the retina[30–32]) where it plays a well-established role in emmetropization.[33,34] Therefore we checked NO-generating pathways among the significantly affected canonical signaling pathways identified using Qiagen IPA (Supplementary Table S1). Three NO-generating pathways are affected significantly more in albinos than in pigmented GPs; these are: the endothelial NOS (eNOS, NOS3) signaling pathway ($P = 0.007$, z-score = 1.4, ranked 87), the neuronal NOS (nNOS, NOS1) signaling pathway ($P = 0.03$, ranked 144), and NO signaling in the cardiovascular system (NOS1-, NOS2-, and NOS3-related) ($P = 0.003$, z-score = 1.4, ranked 65). Proteins involved in these three canonical pathways are listed in Table 4 (with the proteins shared in all three pathways in bold). The differences in protein levels between albino and pigmented choroid suggest that the production of NO in the choroid in albino and pigmented GPs could be different; however, the assay used herein measured only the protein amounts, not the activity, of those enzymes. Other key proteins could be members of the protein kinase C family, given its involvement in all four canonical pathways mentioned above.

## Discussion

### Main Results and Significance of Current Study

The current study demonstrated that choroidal development is genetically controlled, at least in part, in our guinea pigs, which is consistent with observations in humans[35] and selectively-bred chicks.[17] Our results also demonstrated that ChT early in life may predict the susceptibility of eye growth to myopiagenesis in GPs. This correlation was particularly apparent for the pigmented GP strain, perhaps because of a ceiling effect among the albino GP strain, which had thinner ChT overall. The process of choroidal thickening might be influenced by NO-dependent cell-cell signaling in the retina (which is avascular in GP),[30] along the retina-RPE-choroid pathway,[36] or more directly by a functional NO system in the choroid[37] comprising eNOS-containing vascular endothelial cells and nNOS-containing parasympathetic nerve fibers that innervate them.[38,39] Thus it could be a key component of the growth-regulating pathways that pass signals from the retina to the sclera, and the underlying mechanism could relate to dysfunction of the choroidal vascular system.

At present, GPs are being widely used as animal models of myopia. Most results related to experimentally induced

Table 4. NO-Related Canonical Pathways Identified by IPA Bioinformatic Software and Gene Names of Involved Proteins Found By Proteomics Analysis With Their Fold Change

| Affected NO-Related Pathways | NO Signaling in the Cardiovascular System | eNOS Signaling | nNOS Signaling in Neurons |
|---|---|---|---|
| Gene names of significantly involved proteins and their fold change in albino choroid vs. pigmented choroid | *AKT3* (1.5)<br>*ATP2A1* (0.5)<br>*CACNA2D2* (1.8)<br>*GUCY1A1* (2)<br>*HSP90B1* (0.3)<br>*PRKAG1* (1.6)<br>***PRKCD* (0.7)**<br>***PRKCE* (2.2)**<br>***PRKCQ* (3.5)** | *AKT3* (1.5)<br>*AQP1* (0.6)<br>*GUCY1A1* (2)<br>*HSP90B1* (0.3)<br>*HSPA2* (0.6)<br>*HSPA9* (1.7)<br>*PRKAG1* (1.6)<br>***PRKCD* (0.7)**<br>***PRKCE* (2.2)**<br>***PRKCQ* (3.5)** | *CAPN5* (0.4)<br>***PRKCD* (0.7)**<br>***PRKCE* (2.2)**<br>***PRKCQ* (3.5)** |

myopia in GPs are comparable to those in other mammalian models, and even to those in the more widely used chick models. Moreover, our findings support the results of our previous report[14]—that spontaneous myopia consistently occurs in some strains of GPs, whereas other strains are less susceptible to myopia induction. Therefore, exploring the variety of eye growth phenotypes in this species could enable us to better understand the differences in refraction and incidence of myopia among different human ethnic and geographic populations.

## Differences from Studies in Chicks

Although it was first demonstrated in chickens that the choroid actively changes thickness in experimentally induced myopic eye growth,[4,5] subsequent comparison between growth responses in different strains of chickens showed that induced changes in corneal curvature could also contribute to the induced differences in refractive development. In view of the large variability of ChT in incubator-hatched chicks, studies were conducted within strain, and these showed that initial ChT predicted ocular growth in normal chicks, but not in chick eyes with experimentally altered growth.[17,18] Recently, we reported that two strains of pigmented GPs responded differently to the same myopiagenic stimuli and that this was correlated with the differences in initial ChT.[14] We have built on those foundations in the present work, expanding the study to include an albino strain of GPs and to compare the development of refraction and ChT in two different GP strains (albino and pigmented). The demonstrated association between early ChT and subsequent refractive development, in a longitudinal study design, allowed us further to hypothesize a role for the choroid in eye growth, as well as to suggest an underlying molecular basis of this function.

## Failure of the Visual Signaling Cascade from Retina to Choroid

Following accumulated data from research using animal models studying the response of the choroid to the visual signals from the retina, human studies have also demonstrated significant (though small-amplitude) changes of ChT in response to subtle visual manipulation. Read and colleagues initially reported in detail the changes of axial length,[40] which were found later to result from changes of ChT.[41] Of note, Read and colleagues[40,41] mentioned in the same study that there was no significant effect of refractive error on the changes in axial length after exposure to defocus, but they did not show a detailed data analysis. Chiang and colleagues[42] conducted a similar investigation in a small group of human subjects, using a General Linear Model to analyze the ChT at multiple time points and keeping it as a continuous variable; they, too, reported no difference in ChT between emmetropic and myopic groups. Recently, Swiatczak and Schaeffel[43] reported the results of monitoring axial length in emmetropic and myopic human subjects, while viewing optically altered moving images for 30 minutes. These authors found that positive defocus caused less choroidal thickening in myopic eyes than in emmetropic eyes. Further studies by these authors[44] revealed that reading text with inverted contrast caused a reduction of axial length (due to choroidal thickening) in myopic eyes, which was associated with text size.

Dopamine and NO are neurotransmitters in the retina that mediate adaptation-driven changes in retinal functions.[31,45,46] It is speculated that NO acts downstream to the DA mechanism in the retina, and NO is known to be an important regulator of ocular blood flow, as reviewed comprehensively by Schmetterer and Polyak.[29] Therefore our data in Figure 5 may reflect differences in responses of the choroidal NO systems of albino and pigmented GPs to general anesthesia. Moreover, given that the GP retina is avascular, this indicates that any function of the ocular NO system mediated by its vascular regulatory actions (as opposed to effects on neurotransmission and image processing in the retina) would act primarily through the choroidal vasculature. During the 30-minute-long induction time immediately after injection of ketamine/xylazine cocktail, there is expected to be a time-dependent slowing of ocular blood flow,[47] which was reflected in our experiment as the choroidal thinning at 30 minutes. Beyond the 30-minute mark, the choroid would thicken, which would reflect recovered choroidal blood flow, in pigmented GPs. However, the horizontal line (with near-zero slope) from the albino GP data indicated minimal changes of blood flow in the choroid during induction of and recovery from anesthesia. This finding supports the notion that albino GPs have an underdeveloped choroidal vascular system, as shown in Figure 6.

In addition, choroidal melanocytes in pigmented GPs are contacted by nerve endings that contain neuropeptide Y,[48] one function of which is causing vasoconstriction; general anesthesia might block this action, causing vasodilation.[49] Therefore underdevelopment of the choroid in albino GPs could contribute to or result from choroidal failure to respond to signals from the retina.

Investigative Ophthalmology & Visual Science

In summary, results of the current study confirmed that greater thickness of the choroid may provide (or at least precede) protection from or delay in the onset of myopia, whereas lesser thickness was associated with greater susceptibility to spontaneous myopic shift and experimental myopia-induction potentially via the NO system. Our results are consistent with the results of other studies in GPs, which suggest that thinning of the choroid causes a reduction in choroidal blood flow and that this leads to hypoxia which causes scleral expansion.[50]

## Cellular/Molecular Characteristics of the Choroid Relevant to Myopia Development

En face fundus images (Fig. 6) clearly revealed underdevelopment of blood vessels from the middle to outer layers of choroid in albino GPs; thus, the first affected signal transduction could be NO in blood vessels.[51] Two of the canonical pathways identified among the differentially expressed proteins, eNOS signaling pathway and NO signaling pathway in the cardiovascular system, may be activated as indicated by the z-score employed in the IPA Pathways Activity Analysis module. Other canonical pathways affected more in the choroid of albino than of pigmented GPs are listed in Supplementary Table S1. Gene names of proteins involved in the NO system are listed in Table 4. The content of more than half of the proteins involved in these pathways is upregulated in the choroid of albino GPs. In addition, from the list of genes (Table 4), protein kinase C family members may play a pivotal role in all NO related pathways. Based on a large body of prior studies on NOS,[33,36,39,52–59] we speculate that in the albino choroid, the mobilization and activation of such NO-related pathways are in response to the need for promoting choroidal ECM synthesis and angiogenesis, and more, as a result of myopia development. We would propose that activation of the NO system, by prolonged myopia induction in pigmented GPs or in naturally occurring myopia in albino GPs, could be a compensatory response to protect the eye from accelerated growth.

## Potential Cell Carriers of the Signaling Molecules

NO is multifunctional,[60] and it is therefore of interest to identify the best cellular target(s) of NO signaling—both for treating various ocular diseases and for selecting methods of drug delivery—especially when NO and other agents are strongly implicated in regulation of myopic eye growth.[33,34,55,56,61] Consequently, further work is warranted to understand the roles and mechanisms of choroidal NO signaling in myopic eye growth.

Given that melanocytes are involved in choroidal vascular development,[62] it is not surprising that the choroid is consistently thinner in albinos than in pigmented strains. In addition to producing melanin, melanocytes are also able to secrete a number of signaling molecules in response to ultraviolet radiation and other stimuli.[63] One such signaling substance is nitric oxide (NO); not only have melanocytes from skin been found to produce NO,[64] but also iNOS expression was detected in uveal melanoma,[65] and eNOS has been detected immunohistochemically in human melanocytes.[66] Because the number of melanocytes and the level of melanin synthesis are undeniably below normal in the choroid of albino animals,[62] it is reasonable to speculate that the inferred reduction of choroidal NO production in albinos is due to the deficiencies in number and function of choroidal melanocytes.

Our study is not without its limitations. One of these is that an effect of cycloplegia on choroidal thickness, if it exists, might differ between albino and pigmented GPs, or differ between before and after two weeks of FDM. Fortunately, these effects would have been statistically accounted for through our use of regression analysis. Any effect on albino GPs would be similar in all GPs that underwent OCT measurement and similar for all pigmented GPs. It is also important to note that another limitation is that we employed proteomics in a targeted attempt to test our focused hypothesis that NOS and NO-synthesis play key roles in our GP model of myopia. Given that many other pathways were suggested by our proteomics analysis, future studies and analyses would be needed to elucidate all pathways relevant to myopia, beyond our NOS-focused hypothesis.

## Conclusion: Inspiration for Clinical Application

To improve the prevention of myopia onset and decrease the progression in human children, it is critical to establish an objective evaluation system for predicting and monitoring myopia progression, especially given the difficulties faced with preventing its onset. Thickness of the choroid could be a more reliable marker than axial dimensions (such as VCD and AL) for monitoring the risk of myopia onset and progression in the early stages of postnatal eye development, since the choroid is already significantly thin at P6 in GPs that are susceptible to developing myopia. At P14, VCDs were different, whereas ALs were not; this might be due to the lack of significant choroidal thickening with age in albino GPs, as shown in Figure 2A. Therefore it could be clinically useful to monitor choroidal development as early as possible. Because the dendritic melanocytes extend across the entire choroid, from its inner to outer margins, it would be beneficial to monitor melanin accumulation in the fundus (which should reflect melanocyte activity as well, e.g., by polarization-sensitive OCT). Clearly, more information needs to be known about the biology of choroidal melanocytes in GPs and other models to understand their potential role(s) in emmetropization, myopiagenesis, and other normal and pathological conditions of the eye. Finally, once therapeutic targets related to choroidal thickening are clearly identified, novel drug therapy could be pursued to retard myopia onset or progression in humans. Given the direct exposure of choroid (and thus the retina-RPE-sclera relay process) to the systemic circulation, choroid-targeted therapy might readily be done through injection or even oral administration.

### *Acknowledgments*

The authors thank William K. Stell for his critical and inspirational comments and thorough editing of this manuscript. We would also like to thank Sherlyn Seah for her editorial assistance during the manuscript preparation and revision.

Supported by BMRC/IAF-ICP/JJVC_2019(VAB), SNEC/HREF/2018/0618-8 (LJ) and SingHealth Duke-NUS Academic Medicine Research Grant (AM-SU048-2020 to LJ).

Disclosure: **L. Jiang,** None; **X. Liu,** None; **L. Zhou,** None; **J.M.F. Busoy,** None; **M.T. Khine,** None; **Y.S. Dan,** None; **M. Ke,** None; **N.A. Brennan**, Johnson & Johnson Vision (E); **K.J.V. Catbagan,** None; **L. Schmetterer,** None; **V.A. Barathi,** None; **Q.V. Hoang,** None

## References


1. Wallman J, Winawer J. Homeostasis of eye growth and the question of myopia. *Neuron.* 2004;43:447–468.
2. Nickla DL, Wallman J. The multifunctional choroid. *Prog Retin Eye Res.* 2010;29:144–168.
3. Brown JS, Flitcroft DI, Ying GS, et al. In vivo human choroidal thickness measurements: evidence for diurnal fluctuations. *Invest Ophthalmol Vis Sci.* 2009;50:5–12.
4. Wildsoet C, Wallman J. Choroidal and scleral mechanisms of compensation for spectacle lenses in chicks. *Vision Res.* 1995;35:1175–1194.
5. Wallman J, Wildsoet C, Xu A, et al. Moving the retina: choroidal modulation of refractive state. *Vision Res.* 1995;35:37–50.
6. Chakraborty R, Read SA, Collins MJ. Monocular myopic defocus and daily changes in axial length and choroidal thickness of human eyes. *Exp Eye Res.* 2012;103:47–54.
7. Chakraborty R, Read SA, Collins MJ. Hyperopic defocus and diurnal changes in human choroid and axial length. *Optom Vis Sci.* 2013;90:1187–1198.
8. Read SA, Fuss JA, Vincent SJ, Collins MJ, Alonso-Caneiro D. Choroidal changes in human myopia: insights from optical coherence tomography imaging. *Clin Exp Optom.* 2019;102:270–285.
9. Hoseini-Yazdi H, Vincent SJ, Read SA, Collins MJ. Astigmatic defocus leads to short-term changes in human choroidal thickness. *Invest Ophthalmol Vis Sci.* 2020;61(8):48.
10. Aleman AC, Wang M, Schaeffel F. Reading and Myopia: Contrast Polarity Matters. *Sci Rep.* 2018;8:10840.
11. Lou L, Ostrin LA. Effects of narrowband light on choroidal thickness and the pupil. *Invest Ophthalmol Vis Sci.* 2020;61(10):40.
12. Wallman J, Gottlieb MD, Rajaram V, Fugate-Wentzek LA. Local retinal regions control local eye growth and myopia. *Science.* 1987;237(4810):73–77.
13. Nickla DL. Transient increases in choroidal thickness are consistently associated with brief daily visual stimuli that inhibit ocular growth in chicks. *Exp Eye Res.* 2007;84:951–959.
14. Jiang L, Garcia MB, Hammond D, Dahanayake D, Wildsoet CF. Strain-dependent differences in sensitivity to myopia-inducing stimuli in guinea pigs and role of choroid. *Invest Ophthalmol Vis Sci.* 2019;60:1226–1233.
15. Marzani D, Wallman J. Growth of the two layers of the chick sclera is modulated reciprocally by visual conditions. *Invest Ophthalmol Vis Sci.* 1997;38:1726–1739.
16. Chen YP, Prashar A, Erichsen JT, To CH, Hocking PM, Guggenheim JA. Heritability of ocular component dimensions in chickens: genetic variants controlling susceptibility to experimentally induced myopia and pretreatment eye size are distinct. *Invest Ophthalmol Vis Sci.* 2011;52:4012–4020.
17. Guggenheim JA, Chen YP, Yip E, et al. Pre-treatment choroidal thickness is not predictive of susceptibility to form-deprivation myopia in chickens. *Ophthalmic Physiol Opt.* 2011;31:516–528.
18. Nickla DL, Totonelly K. Choroidal thickness predicts ocular growth in normal chicks but not in eyes with experimentally altered growth. *Clin Exp Optom.* 2015;98:564–570.
19. Xiong S, He X, Deng J, et al. Choroidal thickness in 3001 Chinese children aged 6 to 19 years using swept-source OCT. *Sci Rep.* 2017;7:45059.
20. Read SA, Collins MJ, Vincent SJ, Alonso-Caneiro D. Choroidal thickness in childhood. *Invest Ophthalmol Vis Sci.* 2013;54:3586–3593.
21. Wakatsuki Y, Shinojima A, Kawamura A, Yuzawa M. Correlation of aging and segmental choroidal thickness measurement using swept source optical coherence tomography in healthy eyes. *PLoS One.* 2015;10(12):e0144156.
22. Hansen MH, Kessel L, Li XQ, Skovgaard AM, Larsen M, Munch IC. Axial length change and its relationship with baseline choroidal thickness - a five-year longitudinal study in Danish adolescents: the CCC2000 eye study. *BMC Ophthalmol.* 2020;20(1):152.
23. Jin P, Zou H, Zhu J, et al. Choroidal and retinal thickness in children with different refractive status measured by swept-source optical coherence tomography. *Am J Ophthalmol.* 2016;168:164–176.
24. Bulut A, Oner V, Buyuktarakci S, Kaim M. Associations between choroidal thickness, axial length and spherical equivalent in a paediatric population. *Clin Exp Optom.* 2016;99:356–359.
25. Jiang L, Long K, Schaeffel F, et al. Disruption of emmetropization and high susceptibility to deprivation myopia in albino guinea pigs. *Invest Ophthalmol Vis Sci.* 2011;52:6124–6132.
26. Howlett MH, McFadden SA. Form-deprivation myopia in the guinea pig (Cavia porcellus). *Vision Res.* 2006;46(1-2):267–283.
27. Liu X, Jiang L, Ke M, Schmetterer L, Barathi VA. Using image data to numerically correct the jitter in polarization depth encoding PS-OCT. *Opt Lett.* 2021;46:1692–1695.
28. Kammers K, Cole RN, Tiengwe C, Ruczinski I. Detecting Significant Changes in Protein Abundance. *EuPA Open Proteom.* 2015;7:11–19.
29. Schmetterer L, Polak K. Role of nitric oxide in the control of ocular blood flow. *Prog Retin Eye Res.* 2001;20:823–847.
30. Pottek M, Schultz K, Weiler R. Effects of nitric oxide on the horizontal cell network and dopamine release in the carp retina. *Vision Res.* 1997;37(9):1091–1102.
31. Tekmen-Clark M, Gleason E. Nitric oxide production and the expression of two nitric oxide synthases in the avian retina. *Vis Neurosci.* 2013;30(3):91–103.
32. Shi Q, Teves MM, Lillywhite A, Pagtalunan EB, Stell WK. Light adaptation in the chick retina: Dopamine, nitric oxide, and gap-junction coupling modulate spatiotemporal contrast sensitivity. *Exp Eye Res.* 2020;195:108026.
33. Nickla DL, Wilken E, Lytle G, Yom S, Mertz J. Inhibiting the transient choroidal thickening response using the nitric oxide synthase inhibitor l-NAME prevents the ameliorative effects of visual experience on ocular growth in two different visual paradigms. *Exp Eye Res.* 2006;83:456–464.
34. Nickla DL, Lee L, Totonelly K. Nitric oxide synthase inhibitors prevent the growth-inhibiting effects of quinpirole. *Optom Vis Sci.* 2013;90:1167–1175.
35. Sardell RJ, Nittala MG, Adams LD, et al. Heritability of Choroidal Thickness in the Amish. *Ophthalmology.* 2016;123:2537–2544.
36. Nickla DL, Damyanova P, Lytle G. Inhibiting the neuronal isoform of nitric oxide synthase has similar effects on the compensatory choroidal and axial responses to myopic defocus in chicks as does the non-specific inhibitor L-NAME. *Exp Eye Res.* 2009;88:1092–1099.
37. Summers JA, Martinez EC. Visually induced changes in cytokine production in the chick choroid. *Elife.* 2021;10:e70608.
38. Lutjen-Drecoll E. Choroidal innervation in primate eyes. *Exp Eye Res.* 2006;82:357–361.
39. Yu T, Xie X, Wei H, et al. Choroidal changes in lens-induced myopia in guinea pigs. *Microvasc Res.* 2021;138:104213.
40. Read SA, Collins MJ, Sander BP. Human optical axial length and defocus. *Invest Ophthalmol Vis Sci.* 2010;51:6262–6269.
41. Read SA, Alonso-Caneiro D, Vincent SJ, Collins MJ. Longitudinal changes in choroidal thickness and eye growth in childhood. *Invest Ophthalmol Vis Sci.* 2015;56:3103–3112.

42. Chiang ST, Phillips JR, Backhouse S. Effect of retinal image defocus on the thickness of the human choroid. *Ophthalmic Physiol Opt.* 2015;35:405–413.
43. Swiatczak B, F Schaeffel. Emmetropic, but not myopic human eyes distinguish positive defocus from calculated blur. *Invest Ophthalmol Vis Sci.* 2021;62(3): 14.
44. Swiatczak B, Schaeffel F. Transient eye shortening during reading text with inverted contrast: effects of refractive error and letter size. *Transl Vis Sci Technol.* 2022;11(4): 17.
45. Witkovsky P. Dopamine and retinal function. *Doc Ophthalmol.* 2004;108(1):17–40.
46. Jackson CR, Ruan GX, Aseem F, et al. Retinal dopamine mediates multiple dimensions of light-adapted vision. *J Neurosci.* 2012;32:9359–9368.
47. Moult EM, Choi W, Boas DA, et al. Evaluating anesthetic protocols for functional blood flow imaging in the rat eye. *J Biomed Opt.* 2017;22(1):16005.
48. Bruun A, Ehinger B, Sundler F, Tornqvist K, Uddman R. Neuropeptide Y immunoreactive neurons in the guinea-pig uvea and retina. *Invest Ophthalmol Vis Sci.* 1984;25:1113–1123.
49. Masamoto K, Kanno I. Anesthesia and the quantitative evaluation of neurovascular coupling. *J Cereb Blood Flow Metab.* 2012;32:1233–1247.
50. Wu H, Chen W, Zhao F, et al. Scleral hypoxia is a target for myopia control. *Proc Natl Acad Sci USA.* 2018;115(30):E7091–E7100.
51. Knowles RG, Moncada S. Nitric oxide as a signal in blood vessels. *Trends Biochem Sci.* 1992;17:399–402.
52. Das Evcimen N, King GL. The role of protein kinase C activation and the vascular complications of diabetes. *Pharmacol Res.* 2007;55:498–510.
53. Wu J, Liu Q, Yang X, Yang H, Wang XM, Zeng JW. Time-course of changes to nitric oxide signaling pathways in form-deprivation myopia in guinea pigs. *Brain Res.* 2007;1186:155–163.
54. Fujikado T, Kawasaki Y, Fujii J, et al. The effect of nitric oxide synthase inhibitor on form-deprivation myopia. *Curr Eye Res.* 1997;16:992–996.
55. Carr B, Stell WK. Nitric oxide (NO) mediates the inhibition of form-deprivation myopia by atropine in chicks. *Sci Rep.* 2016;6(1):9.
56. Fujikado T, Tsujikawa K, Tamura M, Hosohata J, Kawasaki Y, Tano Y. Effect of a nitric oxide synthase inhibitor on lens-induced myopia. *Ophthalmic Res.* 2001;33:75–79.
57. Murphy MJ, Crewther DP, Goodyear MJ, Crewther SG. Light modulation, not choroidal vasomotor action, is a regulator of refractive compensation to signed optical blur. *Br J Pharmacol.* 2011;164:1614–1626.
58. Nickla DL, Wildsoet CF. The effect of the nonspecific nitric oxide synthase inhibitor NG-nitro-L-arginine methyl ester on the choroidal compensatory response to myopic defocus in chickens. *Optom Vis Sci.* 2004;81:111–118.
59. Tkatchenko TV, Troilo D, Benavente-Perez A, Tkatchenko AV. Gene expression in response to optical defocus of opposite signs reveals bidirectional mechanism of visually guided eye growth. *PLoS Biol.* 2018;16(10):e2006021.
60. Förstermann U, Sessa WC. Nitric oxide synthases: regulation and function. *Eur Heart J.* 2012;33(7):829–837, 837a-837d.
61. Carr B, Stell WK. The science behind myopia. In: Kolb H, Fernandez E, Nelson R . (eds.), *Webvision: The Organization of the Retina and Visual System 2017 edn*. Salt Lake City, UT: University of Utah Health Sciences Center, 1995. 2017.
62. Shibuya H, Watanabe R, Maeno A, et al. Melanocytes contribute to the vasculature of the choroid. *Genes Genet Syst.* 2018;93:51–58.
63. Hu DN, Savage HE, Roberts JE. Uveal melanocytes, ocular pigment epithelium, and Muller cells in culture: in vitro toxicology. *Int J Toxicol.* 2002;21:465–472.
64. Tsatmali M, Graham A, Szatkowski D, et al. Alpha-melanocyte-stimulating hormone modulates nitric oxide production in melanocytes. *J Invest Dermatol.* 2000;114:520–526.
65. Johansson CC, Mougiakakos D, Trocme E, et al. Expression and prognostic significance of iNOS in uveal melanoma. *Int J Cancer.* 2010;126:2682–2689.
66. Bhutto IA, Baba T, Merges C, McLeod DS, Lutty GA. Low nitric oxide synthases (NOSs) in eyes with age-related macular degeneration (AMD). *Exp Eye Res.* 2010;90:155–167.


Investigative Ophthalmology & Visual Science